Theor. Comput. Fluid Dyn.
https://doi.org/10.1007/s00162-024-00727-9

ORIGINAL ARTICLE

Stefano Meloni · Roberto Camussi · Christophe Bogey

An analysis of the effect of the jet initial conditions on the wavelet separated near-field acoustic pressure

Received: 14 June 2024 / Accepted: 9 November 2024

Abstract This paper reports a parametric investigation of the effect of the nozzle exhaust initial conditions on the wavelet separated acoustic pressure generated by a single stream compressible jet in its near field from a database obtained by Large-Eddy Simulations of jet flows at M = 0.9 and Re = 10^5. The nozzle–exit boundary–layer conditions consist of different turbulence intensities for fixed thickness and several thicknesses in laminar conditions. Pressure time series are extracted from virtual probes distributed in the near field of the jets and the acoustic components of the near field pressure are extracted using a wavelet-based procedure able to decontaminate the signals from the hydrodynamic contribution. The reconstructed acoustic time series are analyzed in the frequency domain and in terms of Overall Sound Pressure Level (OASPL). The results show that both the boundary-layer thickness and the turbulence level significantly affect the acoustic pressure in terms of both intensity and directivity. In the laminar case, strong sideline components are observed and strongly depend on the boundary layer thickness. These components clearly appearing in the energy spectra are associated with the Kelvin–Helmholtz instability waves. For large nozzle-exit turbulence intensities, the acoustic field is more uniform and less intense in the sideline direction. On the other hand, the streamwise directivity of the acoustic pressure appears to be strictly correlated to the length of the jet potential core which strongly varies with the initial conditions.

Keywords Jet noise · Acoustic field · Wavelet · LES

1 Introduction

The high-speed flow issuing from the jet exhaust of the propulsive system of modern civil aircraft is known to be one of the main sources of noise during take-off. Since the seminal work of Lighthill [1], many studies have been devoted to identifying the physical mechanisms by which jet turbulent structures generate noise (see e.g. Goldstein [2], Lilley [3], Cavalieri et al. [4]). To the extent of physical understanding and modelling, significant progress has been accomplished recently by the use of a wavepacket source model and by the application of linear stability analysis (see among many: Jordan and Colonius [5], Cavalieri et al. [6], Palma

S. Meloni (✉)
Department of Economics, Engineering, Society and Business Organization, Università della Tuscia, Via Santa Maria in Gradi 4, Viterbo 01100, Italy
E-mail: stefano.meloni@unitus.it

R. Camussi
Department of Civil, Computer Science and Aeronautical Technologies Engineering, Università degli Studi Roma Tre, Via della Vasca Navale 79, Rome 00146, State, Italy

C. Bogey
CNRS, Ecole Centrale de Lyon, INSA Lyon, Universite Claude Bernard Lyon I, Laboratoire de Mécanique des Fluides et d'Acoustique, Ecully UMR 5509, France

Published online: 21 November 2024

et al. [7]). However, despite the indisputable success of these approaches, several aspects still remain unclear and need further investigation.

One of the open questions, that is the subject of the present analysis, concerns the influence of the conditions of the flow at the jet exit on the generation of acoustic waves and their propagation towards the far field. Indeed, according to the literature [8–11], the flow state at the nozzle exhaust plays a key role in the noise emission since it influences relevant physical mechanisms correlated to jet noise generation, such as the laminar-to-turbulent transition of the near wall flow and the flow mixing in the jet plume [12].

Several studies in the literature have shown that, in addition to the Reynolds (Re) and Mach number (M), the main jet-exit flow properties that can be directly correlated to the acoustic emissions are the shear layer momentum thickness, the boundary layer (BL) velocity profile and the turbulence intensity (TI). These parameters are difficult to vary and control in experiments and may vary unexpectedly from one experiment to another even when Re and M are supposed to be the same. Thus, the only way to evaluate quantitatively their efficacy in influencing jet noise is through numerical simulations and this motivated the relevant effort pursued in this field during the last decades [10,11,13–19]. The investigations can be reflected in the careful design of the nozzle shape, which aims to achieve a desired flow state and minimise noise emissions. This can be obtained by employing various techniques, such as chevron, elliptic, and tripped nozzles.

This study aims to enhance and expand upon the findings in the existing literature by providing a detailed analysis of the near-acoustic field of a jet, derived from a comprehensive numerical database covering various flow conditions at the exit of a compressible subsonic nozzle. This analysis will enable a thorough characterization of the near-acoustic field, incorporating a broad set of parameters that have not been previously analyzed from an acoustic perspective. As a result, it will offer significant added value to the understanding of the phenomenon. The parametric analysis proposed therein attempts to clarify the sensitivity of the jet acoustic pressure in the near-field upon the initial conditions. Indeed, the investigation is focused on the region close to the jet flow where, as pointed out by Tinney and Jordan [20], the beginnings of sound, destined to become noise in the far field, are contained. Indeed the acoustic near-field plays a pivotal role in shaping the mechanisms that govern noise generation and dispersion, which are essential for accurately predicting and controlling far-field acoustic behavior. The present investigation is based on the post-processing of a large-eddy-simulation (LES) database containing pressure time series covering a domain that varies in the stream-wise direction from x=0 up to x/D=20 and in the radial direction from r/D=0.5 (nozzle line) up to r/D=3, where D is the jet exit diameter. Simulations have been performed by varying the nozzle exhaust turbulence intensity from $TI = 0\%$, which corresponds to a fully laminar case, up to $TI = 15\%$, which is representative of a fully disturbed jet, with a step of ΔTI of 3%. The second parameter explored is the boundary layer thickness δ_{bl}, normalized by the nozzle exhaust radius r_0. Specifically, the value of δ_{bl}/r_0 spans from 0.025 up to 0.4, doubling the value of the thickness at each step, and keeping fixed the nozzle exhaust turbulence intensity at $TI = 0\%$.

It is known that (see e.g. Tinney and Jordan [20], Guj and Camussi [21], Arndt et al. [22], Grizzi and Camussi [23], Mancinelli et al. [24], Jawahar et al. [25], Meloni and Kamliya Jawahar [26]) the near-field pressure contains a propagating acoustic part and a non-propagating hydrodynamic (or pseudo-sound) counterpart, whence the exigence to analyse the two pressure components separately. In this work, the acoustic component of the pressure time series is extracted by applying a procedure well assessed in the literature [24] based on the application of wavelet transform to the pressure data. The decomposed signals are then analyzed separately in terms of statistical quantities in the physical and Fourier domains.

Details on the numerical setup and the wavelet-based processing procedure are given in Sects. 2 and 3 respectively. Main results are reported in Sec. 4 whereas conclusions and final remarks are given in Sec. 5.

2 Numerical setup

Large Eddy Simulations of round free jets at a Reynolds number $Re = 10^5$ and Mach number M=0.9 have been used for the analysis reported in this paper. The Reynolds number and the jet Mach number are defined as follows:

$$Re = \frac{\rho U_j D_j}{\mu} \tag{1}$$

$$M = \frac{U_j}{\sqrt{\gamma R T_a}} \tag{2}$$

Table 1 Jet initial conditions

M	Re_D	TI	δ_{bl}/r_0
0.9	10^5	0	0.15
0.9	10^5	3%	0.15
0.9	10^5	6%	0.15
0.9	10^5	9%	0.15
0.9	10^5	12%	0.15
0.9	10^5	15%	0.15
0.9	10^5	0	0.025
0.9	10^5	0	0.05
0.9	10^5	0	0.1
0.9	10^5	0	0.2
0.9	10^5	0	0.4

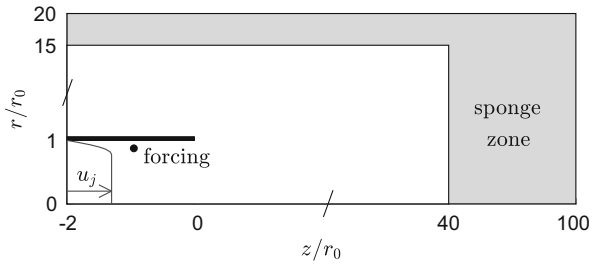

Fig. 1 A sketch of the numerical domain

U_j, D_j, and T_a represent the nozzle exhaust velocity, nozzle exhaust diameter, and the ambient temperature, respectively. Meanwhile, ρ and μ denote the air density and air viscosity, while γ and R are the air gas constants. The jets originate from a short pipe nozzle at the inlet of which a boundary layer velocity profile is prescribed and in which low amplitude disturbances can be added to obtain a non–fully laminar state at the nozzle exit [16,27].

The first set of LES considers jets with a nozzle exhaust boundary layer thickness fixed at $\delta_{bl} = 0.15r_0$. The nozzle exit turbulence intensity has been varied in all the different simulations with a step of $\Delta TI = 3\%$, starting from a fully laminar case with $TI = 0\%$ to the fully disturbed case $TI = 15\%$. These conditions have been achieved by tripping the pipe boundary layers using random low-level vortical disturbances decorrelated in the azimuthal direction (see details in [27], for the analytical procedure of the tripping). A second set of simulations has been carried out with $TI = 0$ and normalized boundary–layer thickness δ_{bl}/r_0 varying from 0.025 up to 0.4 doubling the value of δ_{bl}/r_0 at each step. Given the limited length of the pipe nozzle, in all cases, the BL does not develop and the mean velocity profile at the pipe exit is very similar to the profile prescribed at the inlet. For the sake of clarity, the jet initial conditions are summarized in Table 1.

An in-house solver, based on the three-dimensional filtered compressible Navier–Stokes equations in cylindrical coordinates, has been used to perform the LES simulations. The computational domain is illustrated in Fig. 1 Specifically, the LESs were carried out using grids containing a number of points varying between 250 million and 1 billion, with low-dissipation finite-difference schemes and relaxation filtering as a subgrid-scale dissipation model [27]. The LES are detailed at length in several references [28–30].

The present study is limited to the near-field domain, usually identified as the noise-producing region of the jet flow and thus of interest for jet-noise modelling. Pressure time series are extracted from virtual probes at different locations in the near field, covering a domain that spans from the nozzle exhaust up to $x/D = 20$ in the axial direction and from the nozzle lip line ($r/D = 0.5$) up to $r/D = 3$ in the radial direction. The data set has been acquired at a sampling frequency corresponding to St=12.8 for 3221 time snapshots.

3 Post-Processing Procedure

The data processing relies on separating the acoustic component of the pressure signals from the hydrodynamic counterpart. This goal is achieved by applying the procedure proposed by Grizzi and Camussi [23] and Mancinelli et al. [24], Camussi and Meloni [31] that is briefly worked out in what follows.

The method is based on the wavelet transform of pressure signals and an appropriate filtering of the resulting wavelet coefficients. It is known that the wavelet transform performs well in identifying and isolating intermittent or time-dependent features. For a pressure time series $p(t)$, the wavelet transform can be formally represented by the following expression. [26,32–35]:

$$w(s,t) = C_{\psi}^{-\frac{1}{2}} s^{-\frac{1}{2}} \int_{-\infty}^{\infty} p(\tau)\psi^*\left(\frac{t-\tau}{s}\right)d\tau, \tag{3}$$

where s is the wavelet scale, τ is a time shift, $C_{\psi}^{-\frac{1}{2}}$ is a constant that takes into account the mean value of $\psi(t)$ and $\psi^*\left(\frac{t-\tau}{s}\right)$ is the complex conjugate of the dilated and translated mother wavelet $\psi(t)$.

To perform the acoustic/hydrodynamic separation, the wavelet coefficients can be separated by assuming that the hydrodynamic contribution, being related to localized eddy structures, compresses well onto the wavelet basis so that it originates, in the transformed domain, few but with large amplitude wavelet coefficients. Thus, the so-called pseudo-sound (i.e., the hydrodynamic component of pressure fluctuations) can be extracted by selecting the wavelet coefficients exceeding a proper threshold (see eq. 4). In the present approach, the threshold is identified through the so-called WT3 technique, presented in Mancinelli et al. [24]. The procedure is based on an iterative process originally developed for signal denoising [36] and then applied to the analysis of coherent structures in turbulence [37]. The iterations start from an initial guess evaluated according to the following formula:

$$T = \sqrt{\sigma_k log_{10} N_s} \tag{4}$$

where σ_k is the variance of the (presumed) acoustic pressure at iteration k and N_s is the number of samples. The algorithm stops when the number of selected acoustic wavelet coefficients remains constant between two consecutive iterations. The method is based on single-point statistics. Thus it does not require any additional signals taken from other microphones. Furthermore it has been applied successfully also to configurations out of jet noise (e.g. Li et al. [38], Hajczak et al. [39], Pérez Arroyo et al. [40]). In the present approach, the application of the decomposition procedure provides the reconstruction in the physical domain of the acoustic pressure in the near field of the jet.

Once the wavelet coefficients are separated, the acoustic pressure is reconstructed in the time domain by the inverse transform of the wavelet coefficients having amplitude lower than the threshold and by setting to zero the other wavelet coefficients (i.e. those with amplitude larger than the threshold). Similarly, by setting to zero the coefficients with amplitude lower than the threshold, the hydrodynamic pressure can be recovered.

In summary, the procedure splits a given pressure signal into two time series representing the acoustic and the hydrodynamic pressure components. The two time series are then processed separately and statistical properties are eventually computed.

The properties in the Fourier domain of a decomposed signal are illustrated in Fig. 2 at $x/D = 4$ and $r/D = 1$. It is shown that the hydrodynamic component contains most of the low–frequency energy content of the signal whereas the acoustic pressure is concentrated at higher frequencies. Further results obtained in the Fourier domain are presented in the next section.

4 Flow qualification

This paragraph provides a characterization of the flow exhausting by the various jets considered in terms of vorticity and pressure fields. Figure 3 presents the flow fields of the jets at different nozzle exhaust turbulence intensities. For the case reported in Fig. 3a and b the shear layers are (fully or nominally) laminar in the first axial locations, leading to laminar-turbulent flow transitions dominated by roll-ups and pairings of large-scale, coherent vortical structures. In these cases, well detectable pressure wave propagating in the jet sideline direction is observed. As reported in Fig. 3e and f with increasing nozzle-exit disturbance level, the shear layers tend towards being initially turbulent, which naturally makes vortex roll-up disappear. More interestingly, the

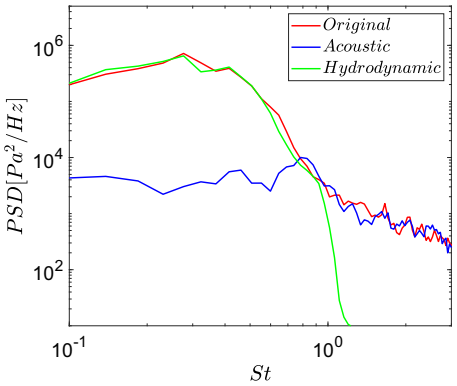

Fig. 2 Decomposed pressure spectra, at x/D = 4 and r/D = 1, for the jet with $TI = 15\%$

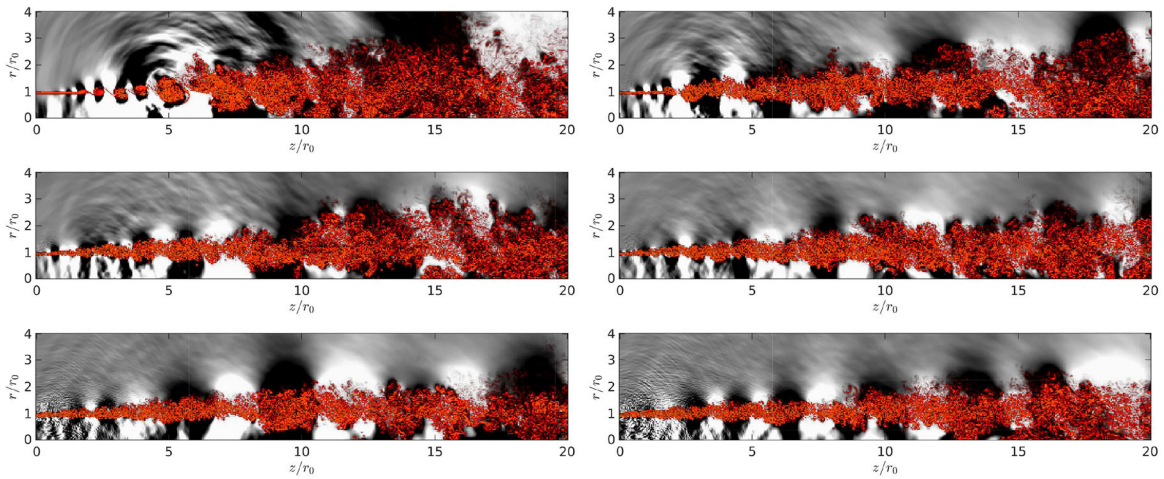

Fig. 3 Representation of vorticity norm and pressure fluctuations obtained for the jets at different nozzle exhaust boundary turbulence intensities: **a** TI = 0%; **b** TI = 3%; **c** TI = 6%; **d** TI = 9%; **e** TI = 12%, **f** TI = 15%. For vorticity, the color scale levels range from 0 to $10u_j/r_0$, from white to red; for pressure, the grey scale levels range between −500 and 500 Pa

mixing layers gradually displays enhanced fine-scale turbulence as well as weaker large-scale structures, and sideline-propagating pressure waves disappear.

Fig. 4 reports the vorticity and pressure fields for the jets with different boundary layer thicknesses. For larger δ_{BL}, vortical structures clearly appear to form more slowly in the shear layers, The rolling-up and vortex pairing occurs farther downstream. The variations of the initial shear-layer thickness also affect the size of the coherent structures generated by the shear-layer rolling-up. As δ_{BL} increases, the structures are significantly larger, as expected.

5 Results

The results are firstly presented in terms of Overall Sound Pressure Level ($OASPL$), which is defined as follows:

$$\mathrm{OASPL} = 20\log_{10}\left(\frac{\sigma}{p_{\mathrm{ref}}}\right), \tag{5}$$

where σ is the standard deviation of the pressure signal and p_{ref} is a reference pressure whose value is $20\mu Pa$.

Figure 5 reports the effects of TI upon the spatial distributions of the $OASPL$ computed from the near–field acoustic pressure, extracted by applying the method outlined in the previous section. A strong acoustic component radiating at angles around 60° with respect to the downstream direction is observed for the laminar and low turbulent cases. It likely results from the fact that, in the laminar case, an effective noise

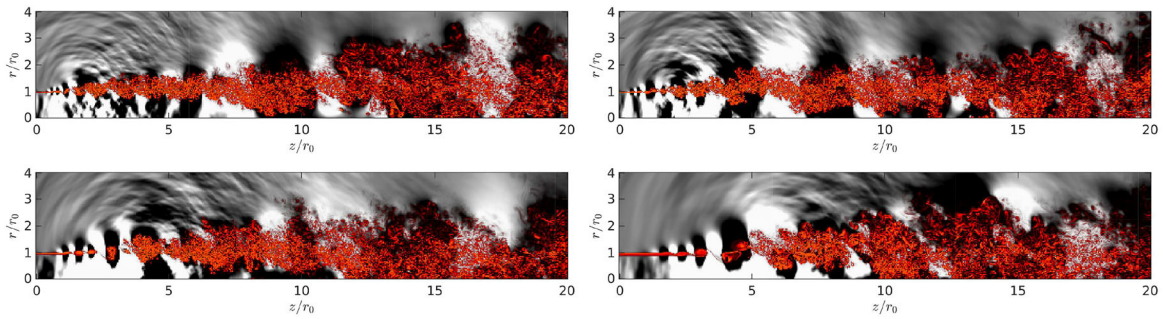

Fig. 4 Representation of vorticity norm and pressure fluctuations obtained for the jets at different nozzle exhaust boundary layer thickness: **a** $\delta_{bl}/r_0 = 0.025$; **b** $\delta_{bl}/r_0 = 0.05$; **c** $\delta_{bl}/r_0 = 0.1$; **d** $\delta_{bl}/r_0 = 0.2$. For vorticity, the color scale levels range from 0 to $10u_j/r_0$, from white to red; for pressure, the grey scale levels range between −500 and 500Pa

generation mechanism is associated with the formation and pairing of vortical structures in the jet shear layer near the nozzle exit, which induces intermittency and radiating sound in preferred directions. This mechanism disappears as TI increases and for turbulence levels larger than 10% (see cases 5 (c) and (f)), the influence of TI on the acoustic near field becomes insignificant.

It is interesting to note that the region close to the jet axis exhibiting a large intensity (the dark red regions of Fig. 5) extends from the nozzle exit between 5 and 10 diameters, depending on the TI. More specifically, for increasing TI, the axial extension increases and reaches about $x/D = 10$ for $TI \geq 9\%$. This behaviour is in agreement with previous analyses [16] and with the flow fields reported in Fig. 3 that shows that an increase of the turbulence intensity leads to a slower development of the shear layers and a longer jet potential core.

Figure 6 reports the OASPL of the acoustic pressure determined at the maximum distance from the jet axis ($r/D = 3$) for the different TI. As was observed in Bogey et al. [16] for the pressure in the far field, the maximum intensity significantly decreases for increasing TI. However, it is observed that for large x/D, corresponding to smaller radition angles, the cases with the highest TI become the noisiest as an effect of the predominance of large-scale contributions.

The effects of the boundary–layer thickness upon the OASPL of the acoustic pressure are reported in Fig. 7. Also in this case, the different initial conditions affect significantly the noise directivity and intensity. For increasing δ_{bl}/r_0, the OASPL pattern in the sideline direction deviates downstream and increases in intensity. This effect might be related to a retarded destabilization of the vortices generated by the roll-up of the shear layer. Indeed, the Kelvin–Helmholtz (K–H) instability waves tend to destabilize at larger x/D for increasing δ_{bl}/r_0.

The region showing high amplitude OASPL close to the jet axis (the dark red regions of Fig. 7) tends to be more concentrated and to have a smaller extension in terms of x/D for increasing BL thickness. As an example, at the lowest δ_{bl}/r_0 (case 7 a), OASPL of the order of 155dB are observed up to x/D of about 15. At the largest thickness (case 7 e), this OASPL amplitude is reached at x/D about 10. This result suggests that a large BL thickness on one side retards the destabilization of the K–H waves but on the other side leads to a more rapid transition to turbulence of the shear layer. Therefore, the extension of the noise-producing region decreases for increasing δ_{bl}/r_0. Furthermore, this trend can also be explained by the decrease of the potential-core length with increasing δ_{bl}/r_0 [15].

In addition to the directivity, the intensity of the acoustic pressure is also significantly affected by the boundary-layer thickness. This is clearly shown in Fig. 8 where the OASPL computed at $r/D = 3$ are reported for the different δ_{bl}/r_0. It is found that the maximum intensity increases for increasing BL thickness whereas for very large x/D the trend is the opposite. As for the TI cases, the acoustic trace at large x/D is related to the large-scale structures and it becomes predominant when the boundary-layer thickness is small.

It is interesting to note that the curves cross at $x/D = 12$ this position representing a transition between two opposite effects. Indeed, for $x/D < 12$, the increase of BL thickness leads to an increase of noise whereas for $x/D > 12$ it leads to a noise diminution. The reason why this transition happens at $x/D = 12$, is related to the delay in the transition to turbulence for higher δ_{bl} as also observed in Fig. 4. Indeed, since the flow at the jet exit is laminar, this transition occurs at a fixed position far downstream the jet orifice, which is strongly affected by the boundary layer thickness.

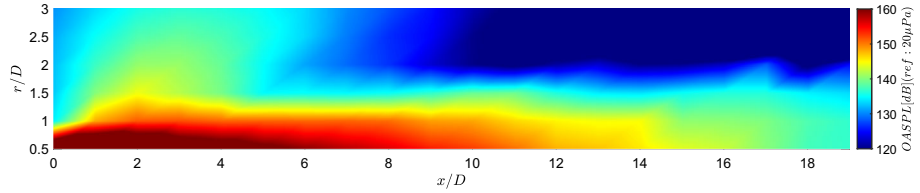

(a)

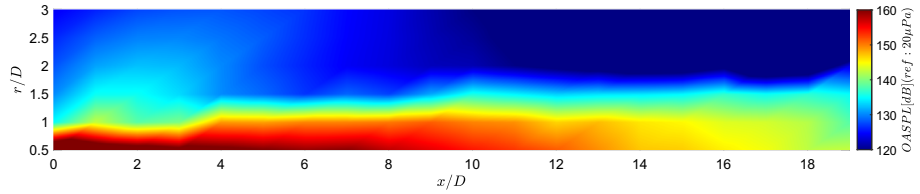

(b)

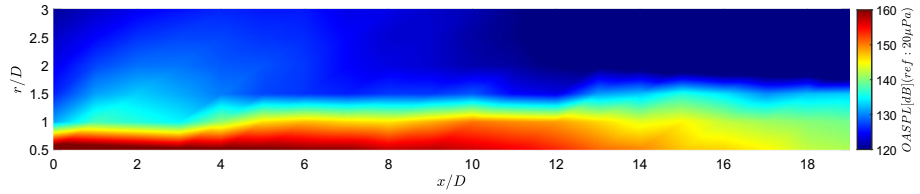

(c)

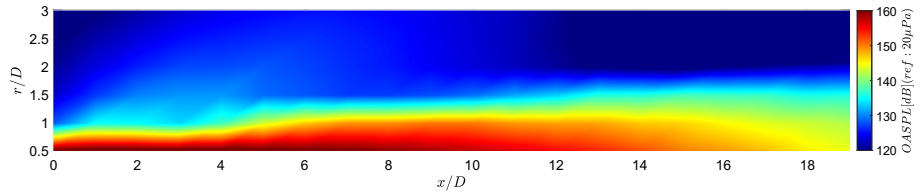

(d)

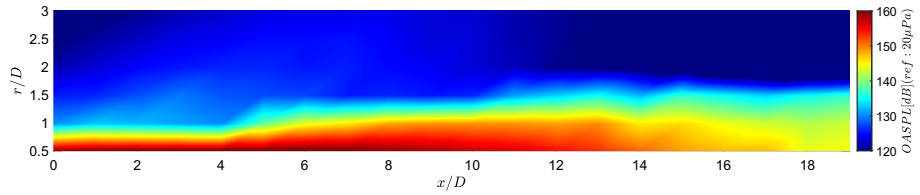

(e)

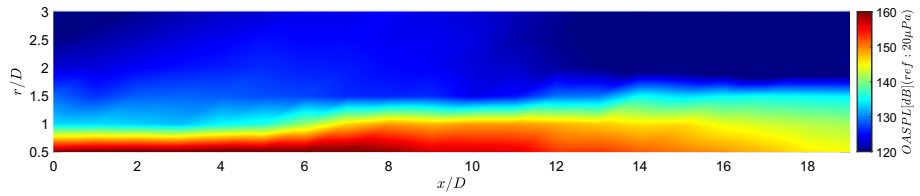

(f)

Fig. 5 OASPL acoustic maps for different nozzle exhaust turbulence intensities: **a** TI = 0%; **b** TI = 3%; **c** TI = 6%; **d** TI = 9%; **e** TI = 12%, **f** TI = 15%

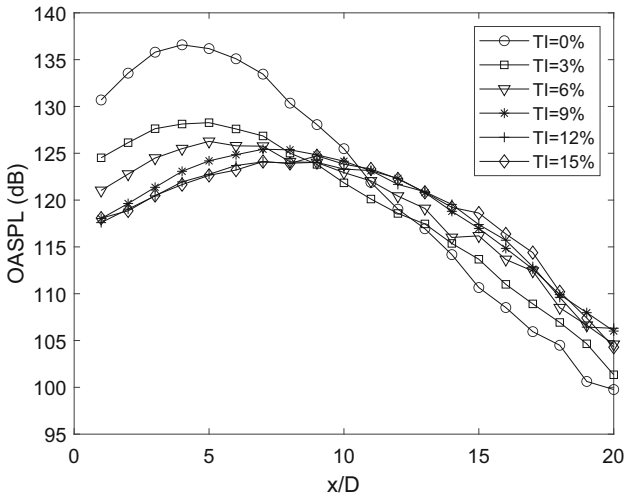

Fig. 6 OASPL of the acoustic pressure at r/D=3 for different TI

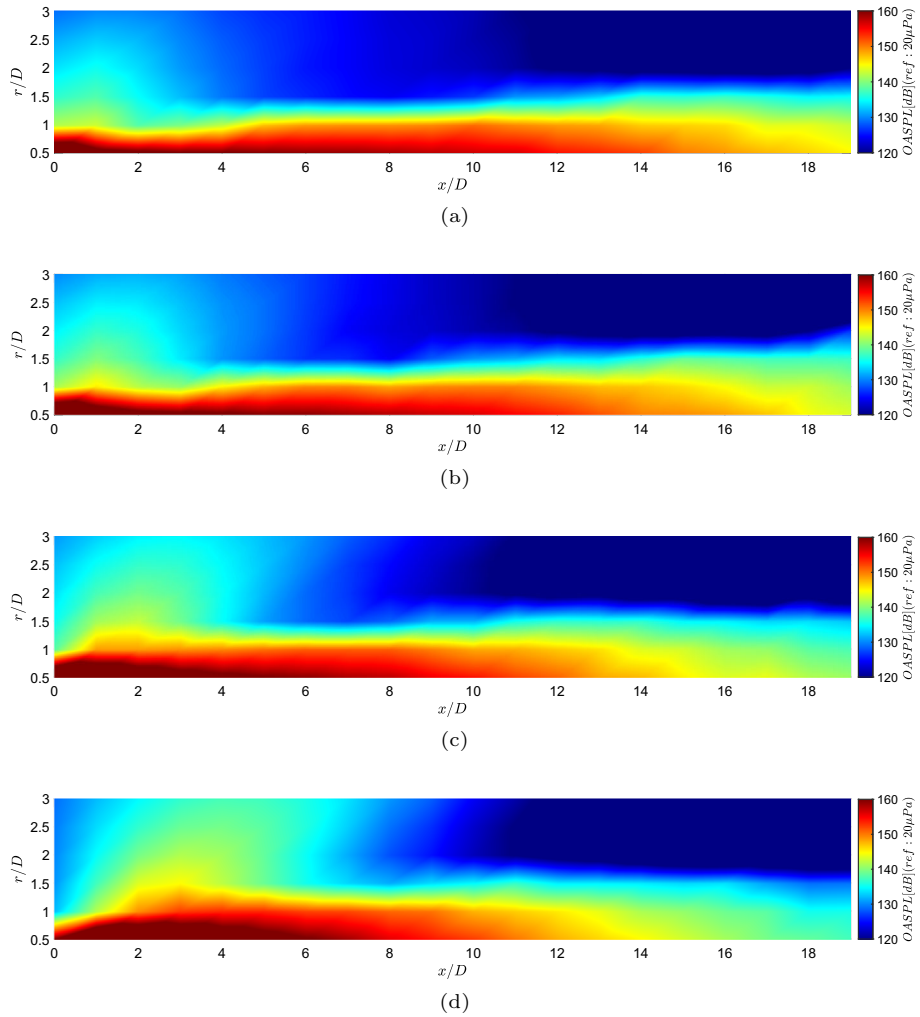

Fig. 7 OASPL acoustic maps for different nozzle exhaust boundary layer thicknesses: **a** $\delta_{bl}/r_0 = 0.025$; **b** $\delta_{bl}/r_0 = 0.05$; **c** $\delta_{bl}/r_0 = 0.1$; **d** $\delta_{bl}/r_0 = 0.2$

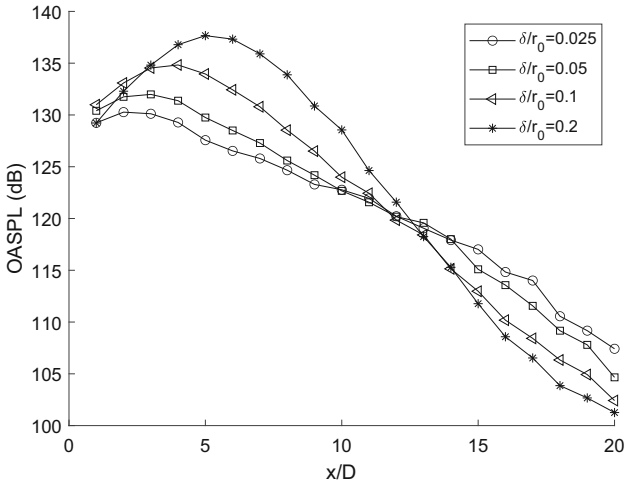

Fig. 8 OASPL of the acoustic pressure at r/D = 3 for different δ_{bl}/r_0

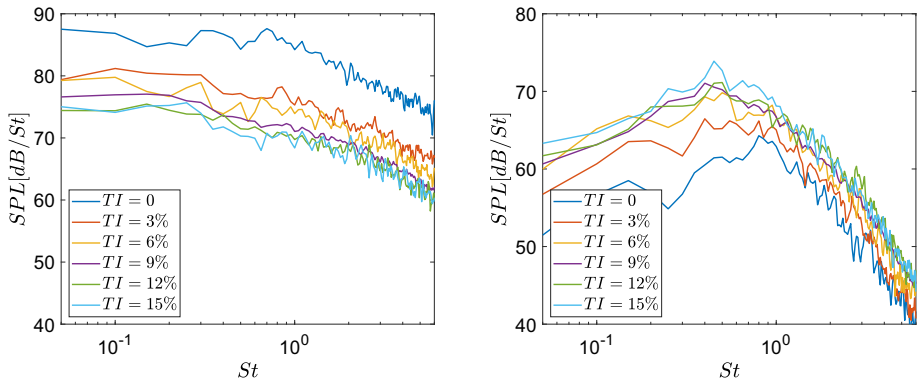

Fig. 9 Frequency spectra computed at $r/D = 3$ for the acoustic component and different TI: **a** at $x/D = 5$; **b** at $x/D = 15$. The spectrum at $TI = 9\%$ is smoother than the other ones due to a higher number of samples

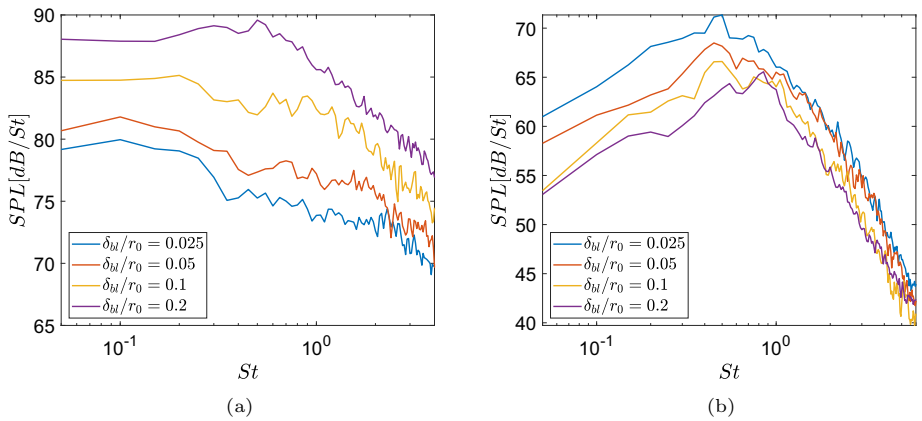

Fig. 10 Frequency spectra computed at $r/D = 3$ for the acoustic component and different BL thicknesses: **a** at $x/D = 5$; **b** at $x/D = 15$

The frequency dependence of the near-field acoustic component is determined through the spectra of the acoustic pressure estimated in terms of the Sound Pressure Level (SPL), given by the following equation:

$$SPL = 10\log_{10}\left(\frac{\mathrm{PSD}\Delta f_{\mathrm{ref}}}{p_{\mathrm{ref}}^2}\right), \tag{6}$$

where PSD denotes the power spectral density evaluated using Welch's method setting Nyquist frequency at St = 12.8, with 256 samples per bin, and applying and Hanning window.

Examples of SPL determined at two different axial positions at $r/D = 3$ ($x/D = 5$ and $x/D = 15$) are given in Figs. 9 and 10, for different turbulence intensities and boundary–layer thicknesses, respectively. Figure 9(a) clearly highlights that at small axial distances, the increase in turbulence intensity leads to a decrease in spectral energy, in the same manner for all frequencies. The decrease is very small for TI values exceeding 9%, which represents a condition of fully developed turbulence. It is noteworthy that observing the same decay trend across different turbulence intensities confirms the complete absence of hydrodynamic components.

In the SPL results reported in Fig. 9b, an opposite behaviour occurs at x/D=15. In that case, an increase of the initial turbulence level of the jet results in an increase in the acoustic spectral energy content. The decrease is strong at low frequencies whereas at Strouhal numbers larger approximately than 1, the energy content is weakly affected by the TI variation. This result indicates that the turbulence intensity variation affects mostly the large–scale structures, in agreement with the directivity patterns reported in Fig. 5. It is also worth noting that for a laminar exit condition, a bump is observed around $St = 1$. It is related to the roll-up and pairing mechanism of the large–scale structures driving laminar turbulent transition, as the Strouhal number of the most amplified instability waves downstream of the nozzle is equal to 1.9 according to linear stability analysis [41]. As the TI increases, the peak Strouhal number shifts towards lower St. Further discussions on this issue are given in the following.

At $x/D = 5$, Fig. 10a, the boundary–layer thickness variation seems to influence the whole range of frequency. Specifically, the thickening of the boundary layer leads to an increase in acoustic pressure at both low and high frequencies. At x/D=15, Fig. 10b, similarly to the effects of the TI, the boundary–layer thickness variation is more localized at low frequencies. In this case as the boundary–layer thickness increases, the peak of the spectrum shifts towards St=1 due to the variations of the vortex–pairing frequency. It is worth noting that the pairing of vortical structures indeed plays a significant role in the generation and in the directional propagation of sound. This occurs primarily due to the coherent motion of the vortices, which induces unsteady radiating sound in preferred directions.

In order to better highlight the acoustic pressure directivity at specific frequencies, SPL intensity is reported in Figs. 8 and 9, as a function of x/D and r/D and for reference Strouhal numbers. The first one is St=0.3 which is representative of the jet column mode, whereas the second one corresponds approximately to the vortex–paring frequency, and depends on the boundary layer thickness that is closely linked to the thickness of the initial mixing layer [15].

The effect of the TI is reported in Fig. 11. Specifically, two significantly different TIs (0 and 12%) are presented for the jet column mode $St = 0.3$ (cases (a) and (b)) and the vortex–pairing Strouhal number $St = 0.93$ (cases (c) and (d)).

The SPL maps are congruent with the directivity patterns of the OASPL reported in Fig. 6 and an intensity weakening is observed for the higher St. It is interesting to note how the signature observed at $St = 0.3$, even though weaker, persists even in the fully developed turbulence condition. The same does not occur at the vortex–pairing Strouhal number where the sideline trace completely disappears for the highest TI.

A similar behaviour is achieved in Fig. 12 which reports the spatial maps of the SPL computed for two different boundary layer–thicknesses (i.e. $\delta_{bl}/r_0 = 0.05$ and $\delta_{bl}/r_0 = 0.2$). In this case, the Strouhal number related to vortex–pairing depends on the nozzle–exhaust boundary layer thickness. Specifically, it is equal to St=2.8 for $\delta_{bl}/r_0 = 0.05$ and St=0.7 for $\delta_{bl}/r_0 = 0.2$.

It is noteworthy that the SPL maps, depicting the jet column mode (Fig. 12a–b), are characterized by a downstream propagating component. This effect becomes more pronounced for larger values of δ_{bl}/r_0, as observed in case

In the case (c), the SPL map at the Strouhal number related to vortex pairing shows a sideline pattern that is inclined close to 90°. This directivity effect disappears in Fig. 12d, which depicts the SPL map at the Strouhal number relative to the vortex pairing with a larger boundary-layer thickness.

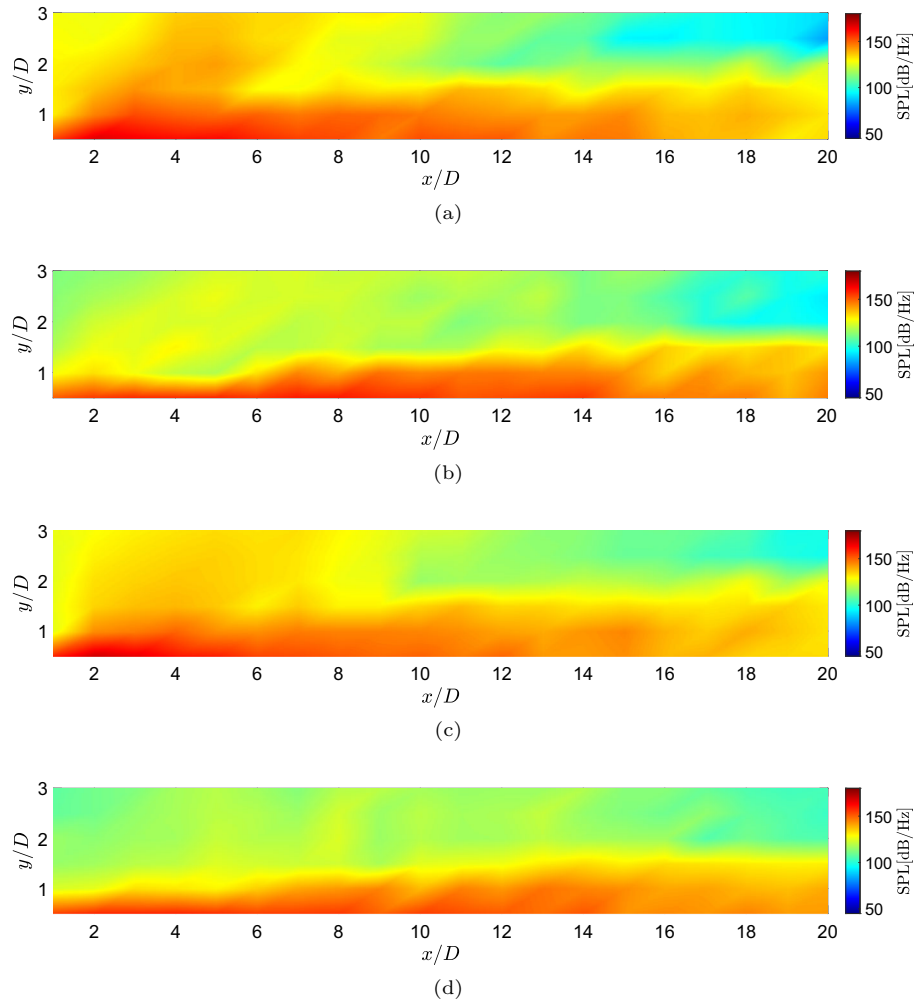

Fig. 11 SPL maps for different Strouhal number and different nozzle exhaust turbulence intensities: **a** $TI = 0$ and St = 0.3; **b** $TI = 12\%$ and St=0.3; **c** $TI = 0$ and St=0.93; **d** $TI = 12\%$ and St = 0.93

6 Conclusions

The present paper reports an analysis of the influence of the nozzle–exit condition of compressible subsonic jets on their near–field acoustic pressure. The investigation is performed by processing a database obtained by well-resolved LES at fixed Mach and Reynolds numbers. The initial conditions are modified by considering different turbulence intensities and boundary–layer thicknesses. More specifically, the different TIs are obtained at constant boundary–layer thickness, whereas the cases with different boundary layer thicknesses correspond to laminar conditions. The acoustic pressure component is extracted from the pressure pointwise data by the application of an existing wavelet-based procedure that allows for the reconstruction of the acoustic pressure time series.

The maps of the acoustic OASPL show that the most noisy region is located in the jet potential core, whose length increases with the turbulence level and reduces significantly with the boundary layer thickness.

The OASPL exhibit a strong directivity at approximately 120°, well visible at low TI and large δ_{BL}. A more detailed analysis of the OASPL intensities, reveals that an increase of TI leads to a lowering of the acoustic pressure in the potential core region whereas an opposite trend is observed at larger axial distances, as an effect of the directivity of the noise generated by the large scale structures. The boundary layer thickness variation induces a similar effect on the OASPL intensity since an opposite trend is observed close and far from the jet exit. The OASPL increases significantly with the BL in agreement with the potential core region whereas it decreases for larger than $x/D = 13$.

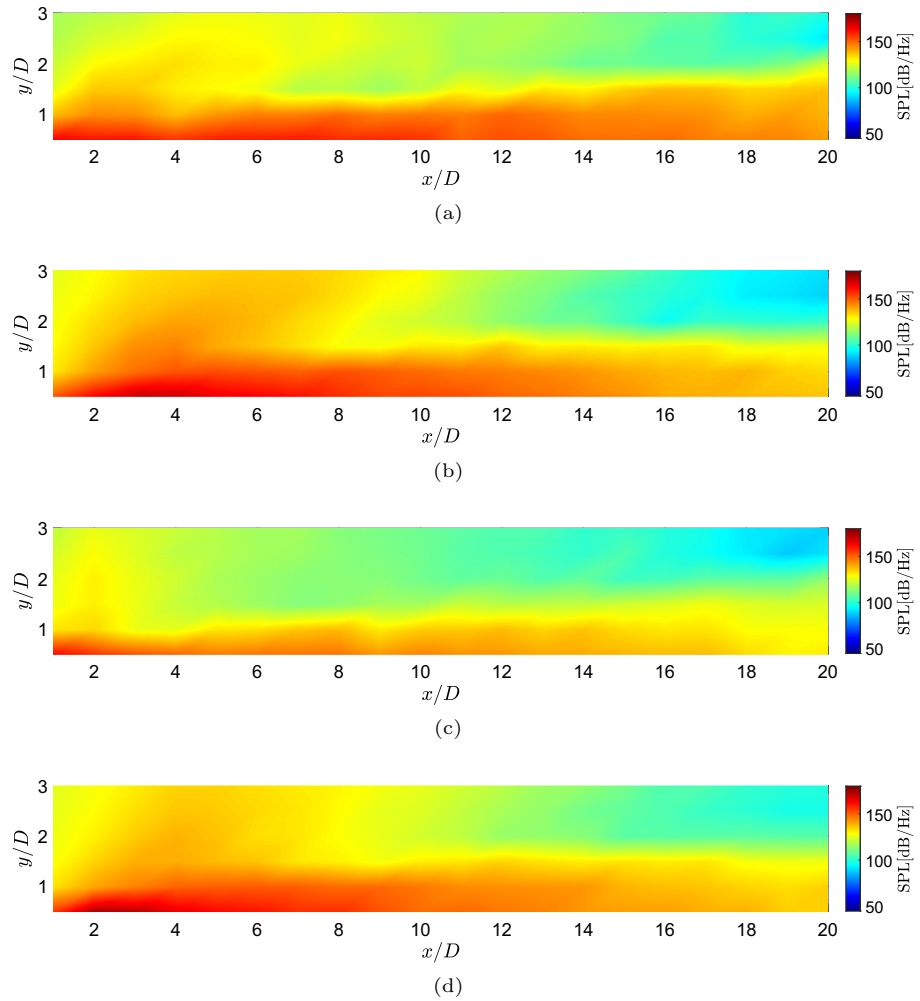

Fig. 12 SPL maps for different Strouhal number and different nozzle exhaust boundary layer thicknesses: **a** $\delta_{bl}/r_0 = 0.05$ and St = 0.3; **b** $\delta_{bl}/r_0 = 0.2$ and St = 0.3; **c** $\delta_{bl}/r_0 = 0.05$ and St=2.8; **d** $\delta_{bl}/r_0 = 0.2$ and St = 0.7

The acoustic spectra, presented in terms of SPL, shed light on the frequency distribution of the energy and thus clarify the way initial conditions influence small or large scales. In the region close to the jet exit, the spectra shape is weakly influenced by both TI and δ_{BL}. An uniform variation of energy content is observed at both small and high frequencies, and an increase of both parameters lead to an increase in energy. At larger x/D the effect is opposite with respect to the small x/D since an increase of both parameters leads to a decrease of energy. On the other hand, the effect is relevant only at small frequencies corresponding to $St < 1$ where the trace of the large-scale structures dynamics is more evident.

The analysis of the acoustic pressure intensity focalized on two specific St related to both the jet column mode and vortex pairing mechanism, emphasizing how the jet initial conditions impact the directional patterns associated with these noise mechanisms.

Further analyses are surely needed in order to develop appropriate models able to predict the effect of the initial conditions on the jet noise. This challenging task will be pursued by the authors in the near future.

Acknowledgements C. Bogey was partially supported by the LABEX CeLyA (ANR-10-LABX-0060/ANR-16-IDEX-0005). The numerical data analyzed in this work were obtained using the HPC resources of PMCS2I (Pôle de Modélisation et de Calcul en Sciences de l'Ingénieur et de l'Information) of Ecole Centrale de Lyon and P2CHPD (Pôle de Calcul Hautes Performances Dédié) of Université Lyon I, and the resources of CINES (Centre Informatique National de l'Enseignement Supérieur) and IDRIS (Institut du Développement et des Ressources en Informatique Scientifique) under the allocation 2023-2a0204 made by GENCI (Grand Equipement National de Calcul Intensif).

Declarations

Author Contribution S.M. Conceptualization, Data curation, Formal analysis, Investigation, Methodology, Writing – original draft, Writing – review and editing; R.C Conceptualization, Methodology, Writing – review and editing; C.B Conceptualization, Data curation, Writing – review and editing

Data Availibility No datasets were generated or analysed during the current study.

Conflict of interest The authors declare no Conflict of interest.

References

1. Lighthill, M.J.: On sound generated aerodynamically. General theory. Proc. R. Soc. Lond. **267**, 564–587 (1952)
2. Goldstein, M.E.: Aeroacoustics of turbulent shear flows. Annu. Rev. Fluid Mech. **16**(1), 263–285 (1984)
3. Lilley, G.M.: On the noise from air jets. AGARD CP **131**, 13–1132 (1974)
4. Cavalieri, A.V.G., Jordan, P., Agarwal, A., Gervais, Y.: Jittering wave-packet models for subsonic jet noise. J. Sound Vib. **330**(18–19), 4474–4492 (2011)
5. Jordan, P., Colonius, T.: Wave packets and turbulent jet noise. Annu. Rev. Fluid Mech. **45**(1), 173–195 (2013)
6. Cavalieri, A.V.G., Jordan, P., Lesshafft, L.: Wave-packet models for jet dynamics and sound radiation. Appl. Mech. Rev. **71**(2), 020802 (2019)
7. Palma, G., Meloni, S., Camussi, R., Iemma, U., Bogey, C.: Data-driven multiobjective optimization of wave-packets for near-field subsonic jet noise. AIAA Journal (2023). https://doi.org/10.2514/1.J062261
8. Gutmark, E., Ho, C.M.: Preferred modes and the spreading rates of jets. Phys. Fluids **26**(10), 2932–2938 (1983)
9. Crighton, D.G.: Acoustics as a branch of fluid mechanics. J. Fluid Mech. **106**, 261–298 (1981)
10. Bogey, C., Sabatini, R.: Effects of nozzle-exit boundary-layer profile on the initial shear-layer instability, flow field and noise of subsonic jets. J. Fluid Mech. **876**, 288–325 (2019). https://doi.org/10.1017/jfm.2019.546
11. Bogey, C., Marsden, O.: Identification of the effects of the nozzle-exit boundary-layer thickness and its corresponding Reynolds number in initially highly disturbed subsonic jets. Phys. Fluids (2013). https://doi.org/10.1063/1.4807071
12. Ho, C., Huerre, P.: Perturbed free shear layers. Annu. Rev. Fluid Mech. **16**(1), 365–422 (1984). https://doi.org/10.1146/annurev.fl.16.010184.002053
13. Bogey, C.: Generation of excess noise by jets with highly disturbed laminar boundary-layer profiles. AIAA J. **59**(2), 569–579 (2021). https://doi.org/10.2514/1.J059610
14. Zaman, K.B.M.Q.: Increased jet noise due to a "nominally laminar" state of nozzle exit boundary layer. In: NASA Report (2017)
15. Bogey, C., Bailly, C.: Influence of nozzle-exit boundary-layer conditions on the flow and acoustic fields of initially laminar jets. J. Fluid Mech. **663**, 507–538 (2010)
16. Bogey, C., Marsden, O., Bailly, C.: Influence of initial turbulence level on the flow and sound fields of a subsonic jet at a diameter-based Reynolds number of 10^5. J. Fluid Mech. **701**, 352–385 (2012). https://doi.org/10.1017/jfm.2012.162
17. Adam, A., Papamoschou, D., Bogey, C.: Imprint of vortical structures on the near-field pressure of a turbulent jet. AIAA J. **60**(3), 1578–1591 (2022). https://doi.org/10.2514/1.J061010
18. Brès, G.A., Jaunet, V., Le Rallic, M., Jordan, P., Colonius, T., Lele, S.K.: Large eddy simulation for jet noise: the importance of getting the boundary layer right. In: 21st AIAA/CEAS Aeroacoustics Conference, AIAA 2015-2535 (2015). https://doi.org/10.2514/6.2015-2535
19. Brès, G.A., Jordan, P., Jaunet, V., Le Rallic, M., Cavalieri, A.V.G., Towne, A., Lele, S.K., Colonius, T., Schmidt, O.T.: Importance of the nozzle-exit boundary-layer state in subsonic turbulent jets. J. Fluid Mech. **851**, 83–124 (2018). https://doi.org/10.1017/jfm.2018.476
20. Tinney, C.E., Jordan, P.: The near pressure field of co-axial subsonic jets. J. Fluid Mech. **611**, 175–204 (2008). https://doi.org/10.1017/S0022112008001833
21. Guj, G., Camussi, R.: Statistical analysis of local turbulent energy fluctuations. J. Fluid Mech. **382**, 1–26 (1999). https://doi.org/10.1017/S0022112098003553
22. Arndt, R.E.A., Long, D.F., Glauser, M.N.: The proper orthogonal decomposition of pressure fluctuations surrounding a turbulent jet. J. Fluid Mech. **340**, 1–33 (1997). https://doi.org/10.1017/S0022112097005089
23. Grizzi, S., Camussi, R.: Wavelet analysis of near-field pressure fluctuations generated by a subsonic jet. J. Fluid Mech. **698**, 93–124 (2012)
24. Mancinelli, M., Pagliaroli, T., Di Marco, A., Camussi, R., Castelain, T.: Wavelet decomposition of hydrodynamic and acoustic pressures in the near field of the jet. J. Fluid Mech. **813**, 716–749 (2017)
25. Jawahar, H.K., Meloni, S., Camussi, R.: Jet noise sources for chevron nozzles in under-expanded condition. Int. J. Aeroacoust. (2022). https://doi.org/10.1177/1475472X221101766
26. Meloni, S., Kamliya Jawahar, H.: A wavelet-based time-frequency analysis on the supersonic jet noise features with chevrons. Fluids (2022). https://doi.org/10.3390/fluids7030108
27. Bogey, C., Marsden, O., Bailly, C.: Large-eddy simulation of the flow and acoustic fields of a Reynolds number 10^5 subsonic jet with tripped exit boundary layers. Phys. Fluids **23**, 035104 (2011)
28. Bogey, C.: Acoustic tones in the near-nozzle region of jets: characteristics and variations between Mach numbers 0.5 and 2. J. Fluid Mech. (2021). https://doi.org/10.1017/jfm.2021.426
29. Bogey, C.: Grid sensitivity of flow field and noise of high-Reynolds-number jets computed by large-eddy simulation. Int. J. Aeroacoust. **17**(4–5), 399–424 (2018). https://doi.org/10.1177/1475472X18778287

30. Bogey, C.: A database of flow and near pressure field signals obtained for subsonic and nearly ideally expanded supersonic free jets using large-eddy simulations. https://hal.archives-ouvertes.fr/hal-03626787 (2022)
31. Camussi, R., Meloni, S.: On the application of wavelet transform in jet aeroacoustics. Fluids **6**(8), 299 (2021)
32. Farge, M.: Wavelet transform and their applications to turbulence. Annu. Rev. Fluid Mech. **24**(1), 395–458 (1992). https://doi.org/10.1146/annurev.fl.24.010192.002143
33. Camussi, R., Robert, G., Jacob, M.C.: Cross-wavelet analysis of wall pressure fluctuations beneath incompressible turbulent boundary layers. J. Fluid Mech. **617**, 11–30 (2008). https://doi.org/10.1017/S002211200800373X
34. Micci, G.L., Camussi, R., Meloni, S., Bogey, C.: Intermittency and stochastic modeling of low-and high-Reynolds-number compressible jets. AIAA J. **60**(3), 1983–1990 (2022). https://doi.org/10.2514/1.J061128
35. Camussi, R., Bogey, C.: Intermittent statistics of the 0-mode pressure fluctuations in the near field of Mach 0.9 circular jets at low and high reynolds numbers. Theoret. Comput. Fluid Dyn. **35**(2), 229–247 (2021)
36. Donoho, D.L., Johnstone, J.M.: Ideal spatial adaptation by wavelet shrinkage. Biometrika **81**(3), 425–455 (1994)
37. Ruppert-Felsot, J., Farge, M., Petitjeans, P.: Wavelet tools to study intermittency: application to vortex bursting. J. Fluid Mech. **636**, 427–453 (2009)
38. Li, S., Rival, D.E., Wu, X.: Sound source and pseudo-sound in the near field of a circular cylinder in subsonic conditions. J. Fluid Mech. **919**, 43 (2021). https://doi.org/10.1017/jfm.2021.404
39. Hajczak, A., Sanders, L., Vuillot, F., Druault, P.: Wavelet-based separation methods assessment on the near pressure field of a landing gear subcomponent. In: 25th AIAA/CEAS Aeroacoustics Conference, p. 2482 (2019). https://doi.org/10.2514/6.2019-2482
40. Pérez Arroyo, C., Daviller, G., Puigt, G., Airiau, C., Moreau, S.: Identification of temporal and spatial signatures of broadband shock-associated noise. Shock Waves **29**(1), 117–134 (2019). https://doi.org/10.1007/s00193-018-0806-4
41. Michalke, A.: Survey on jet instability theory. Prog. Aerosp. Sci. **21**, 159–199 (1984). https://doi.org/10.1016/0376-0421(84)90005-8